Ore Geology Reviews 87 (2017) 114–125

Contents lists available at ScienceDirect

Ore Geology Reviews

journal homepage: www.elsevier.com/locate/oregeorev

Geochemistry and U-series dating of Holocene and fossil marine hydrothermal manganese deposits from the Izu-Ogasawara arc

Kyoko Yamaoka [a,*], Lin Ma [b], Kazuko Hishikawa [c], Akira Usui [a,c]

[a] Geological Survey of Japan, National Institute of Advanced Industrial Science and Technology (AIST), 1-1-1 Higashi, Tsukuba, Ibaraki 305-8567, Japan
[b] Geological Sciences, The University of Texas at El Paso, 500 West University Ave., El Paso, TX 79968, USA
[c] Faculty of Science, Kochi University, 2-5-1 Akebono-cho, Kochi 780-8520, Japan

ARTICLE INFO

Article history:
Received 11 April 2016
Received in revised form 27 July 2016
Accepted 29 July 2016
Available online 26 August 2016

Keywords:
Marine manganese deposit
Hydrothermal activity
U-series age dating

ABSTRACT

This study investigated Holocene and fossil hydrothermal manganese deposits in the Izu-Ogasawara arc. Mineralogically, these deposits comprise 10 Å and 7 Å manganate minerals, and the fossil samples showed higher 10 Å stabilities. Chemical compositions of the Holocene samples are typical of other hydrothermal manganese deposits, including low Fe/Mn ratios, low trace metals, and low rare earth elements. Although the fossil samples generally have similar chemical characteristics, they exhibit significant enrichment in Ni, Cu, Zn, Cd, Ba, REE, Tl, and Pb contents. Furthermore, the chondrite-normalized REE patterns showed more light REE enrichment trends. These chemical characteristics suggest post-depositional uptake of these metals from seawater. U-Th dating of a Holocene hydrothermal manganese deposit from the Kaikata Seamount indicated 8.8 ± 0.94 ka for the uppermost layer and downward growth beneath the seafloor with a growth rate of ca. 2 mm/kyr. This is approximately three orders of magnitude faster than that of hydrogenetic ferromanganese crusts. U-Pb age of a fossil hydrothermal manganese deposit from the Nishi-Jokyo Seamount showed 4.4 ± 1.6 Ma, which was contemporary with basaltic volcanism (5.8 ± 0.3 Ma). Hydrothermal manganese deposits contain high concentrations of high value Mn, but only small amounts of valuable minor metals; their ages constrain the periods of past hydrothermal activity and provide a vector to explore for polymetallic sulfide deposits.

1. Introduction

Manganese oxides in the deep ocean are classified into three types from the perspective of genesis (e.g., Hein, 2004; Usui and Someya, 1997): (1) hydrogenetic ferromanganese crusts/nodules precipitated from ambient seawater, (2) diagenetic manganese nodules precipitated from pore fluids, and (3) hydrothermal manganese deposits precipitated from ascending low-temperature hydrothermal fluids. Hydrothermal manganese deposits are common along the Izu-Ogasawara (Bonin) arc in the northwestern Pacific (Usui and Glasby, 1998; Usui and Someya, 1997). Recent (Holocene) hydrothermal manganese deposits have been found to occur on active seamounts or rifts, whereas "fossil" hydrothermal manganese deposits are found at inactive seamounts. The recent hydrothermal manganese deposits precipitated below the seafloor as stratabound oxide layers and as cement for sediments. The fossil manganese deposits occur as lumps or blocks. They are overlain by hydrogenetic ferromanganese layers.

Previous studies revealed that hydrothermal manganese deposits have distinct chemical, mineralogical, and morphological characteristics. Hydrothermal manganese deposits comprise todorokite (10 Å manganate) and birnessite (7 Å manganate), although it is considered that the 7 Å manganate phase might have transformed from structurally unstable buserite (10 Å manganate) as a result of air drying (Hodkinson et al., 1994; Usui et al., 1989). The chemical compositions of the deposits are characterized by very low Fe/Mn ratios and extremely low contents of most transition metals and rare earth elements. However, some trace elements including Li, Mg, Mo, Zn, Cd, and Ba are occasionally enriched in hydrothermal manganese deposits regarded as indicators of a hydrothermal origin (e.g., Hein et al., 1997; Hodkinson et al., 1994; Kuhn et al., 2003; Moorby et al., 1984; Rogers et al., 2001; Usui and Glasby, 1998). The variations in chemical compositions have been discussed mainly in terms of tectonic settings, whereas the relationship with aging is not fully understood.

Based on limited U-Th age data, very rapid growth rates have been suggested for hydrothermal manganese deposits (Cronan et al., 1982; Hodkinson et al., 1994; Moore and Vogt, 1976; Scott et al., 1974). Although the estimated growth rates (0.1–2 mm/kyr) are fairly consistent, severe inconsistencies exist in growth directions. Scott et al. (1974) and Cronan et al. (1982) demonstrated the older age in the deeper layer (upward growth), whereas Moore and Vogt (1976) and Hodkinson et al. (1994) found opposite trends (downward growth). This difference of findings might be partly attributable to the difficulty in determining the orientation at the seafloor because these deposits were collected

* Corresponding author.
E-mail address: k.yamaoka@aist.go.jp (K. Yamaoka).

http://dx.doi.org/10.1016/j.oregeorev.2016.07.025
0169-1368/

by dredge sampling. Moreover, Burnett and Piper (1977) pointed out that considerable exogenous ^{230}Th derived from detrital materials complicated the application of the U-series dating techniques for hydrothermal manganese deposits. Consequently, detrital correction is necessary to ascertain reliable U-Th ages and to estimate growth rates.

As described in this paper, we present mineralogical and chemical composition data for recent and fossil hydrothermal manganese deposits from active and inactive seamounts, respectively, from the Izu-Ogasawara arc. Similar tectonic settings provide an excellent opportunity to demonstrate the effects of aging on hydrothermal manganese deposits. Additionally, we determined the ages of recent and fossil hydrothermal manganese deposits using U-Th and U-Pb dating techniques, respectively, with detrital correction. The ages and growth rates of hydrothermal manganese deposits provide useful information related to the period and duration of hydrothermal activities. The growth rates of hydrothermal manganese deposits were estimated based on the U-Th ages, whereas the association of past volcanic activity with formation of the manganese deposit was based on U-Pb ages.

2. Sample descriptions

The location, geological setting, and sample description of each hydrothermal manganese deposit are presented in Table 1. According to the classification by Hein et al. (2008), these hydrothermal manganese deposits correspond to stratabound manganese deposits.

2.1. Recent hydrothermal manganese deposits

The recent hydrothermal manganese deposits were collected from the Kaikata Seamount (Smt) and Beyonnaise knoll (Fig. 1). The Kaikata Smt and the Beyonnaise knoll are active submarine volcanoes on the volcanic front (the Shichito-Iwojima Ridge) of the Izu-Ogasawara arc.

The Kaikata Smt has four major peaks: KN, KM, KS, and KC. Hydrothermal activity was observed in the KC caldera. The maximum temperature of discharged water was 33 °C (Tsuchida et al., 2001). Hydrothermal manganese deposits were found on the KN and KM peaks (Usui et al., 1986). They generally extend along a NE–SW trending belt, entirely covering the surface of foraminifera-bearing volcanic sands (Usui and Nishimura, 1992; Usui et al., 1989). Samples (RS-16, RS-18, and RS-48) were collected from the northwestern flank of KM peak during the R/V *Hakurei-maru* cruises in 1985 and 1986 conducted by the Geological Survey of Japan. Sampling was conducted with a camera-mounted rock sampler (a heavy box-core type apparatus that penetrates and recovers 20 cm cores of consolidated deposits). The manganese oxides occur as dense, gray to black, submetallic layers of approximately 20 mm thickness (Fig. 2). These layers are overlain by volcanic sands and/or calcareous ooze layers (5–10 mm thick) with a manganese matrix. The bottom surfaces of RS-16 and RS-18 show

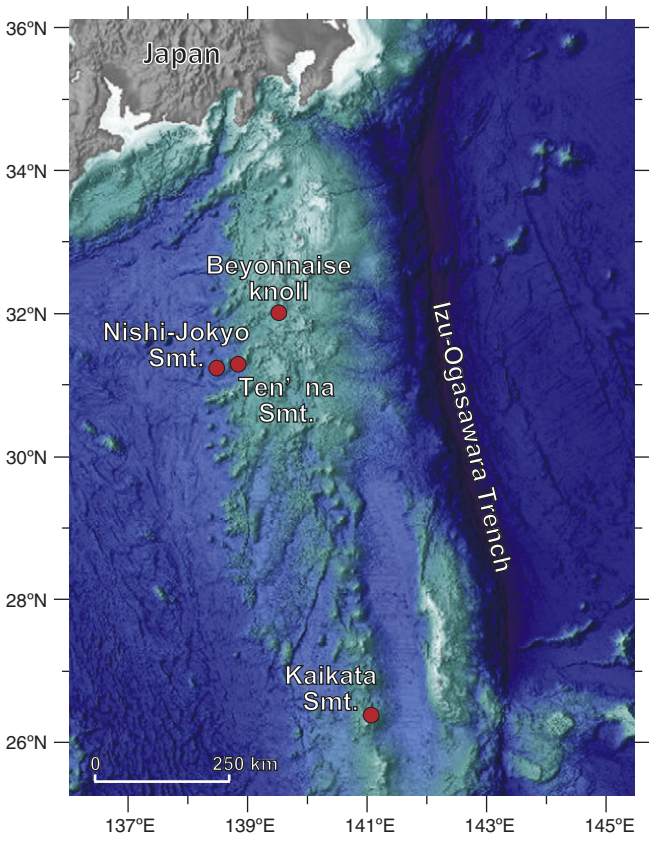

Fig. 1. Location map of active seamounts (Kaikata Smt and Beyonnaise knoll) and inactive seamounts (Nishi-Jokyo Smt and Ten'na Smt) in the Izu-Ogasawara arc.

Table 1
Location, setting, and description of the hydrothermal manganese deposits.

	Recent hydrothermal Mn deposit					Fossil hydrothermal Mn deposit			
Location	Kaikata Seamount			Beyonnaise knoll		Nishi-Jokyo Seamount		Ten'na Seamount	
Area	Shichito-Iwojima Ridge			Shichito-Iwojima Ridge		Nishi-Shichito Ridge		Nishi-Shichito Ridge	
Setting	Frontal volcano			Frontal volcano		Back-arc seamount		Back-arc seamount	
Sample no.	RS-16	RS-18	RS-48	MW D51-X1	6K Dv.611 #1B	MW D19-X2	MW D108-X5	2K Dv.953 St.1#1	MW D103-X21
Latitude (°N)	26.700	26.717	26.685	31.905	31.964	31.307	31.243	31.383	31.360
Longitude (°E)	140.924	140.897	140.916	139.630	139.684	138.388	138.497	138.784	138.852
Water depth (m)	1086	1097	845	1285	1157	1825	2400	1223	1790
Cruise	R/V *Hakurei-maru* cruise in 1985	R/V *Hakurei-maru* cruise in 1986	R/V *Hakurei-maru* cruise in 1986	R/V *Moana Wave* cruise in 1995	Dive *Shinkai 6500* in 1997	R/V *Moana Wave* cruise in 1995	R/V *Moana Wave* cruise in 1995	Dive *Shinkai 2000* in 1997	R/V *Moana Wave* cruise in 1995
Thickness of hydrothermal Mn oxides	20 mm	30 mm	30 mm	10 mm	30 mm	110 mm	40 mm	100 mm	100 mm
Thickness of hydrogenetic Mn oxides	–	–	–	–	–	20 mm	5–10 mm	1 mm	10 mm
Reference	Usui et al. (1986, 1989) Usui and Nishimura (1992)			Iizasa et al. (2004) Tanahashi et al. (2006)		Usui and Glasby (1998)		Usui et al. (1986) Usui and Glasby (1998)	

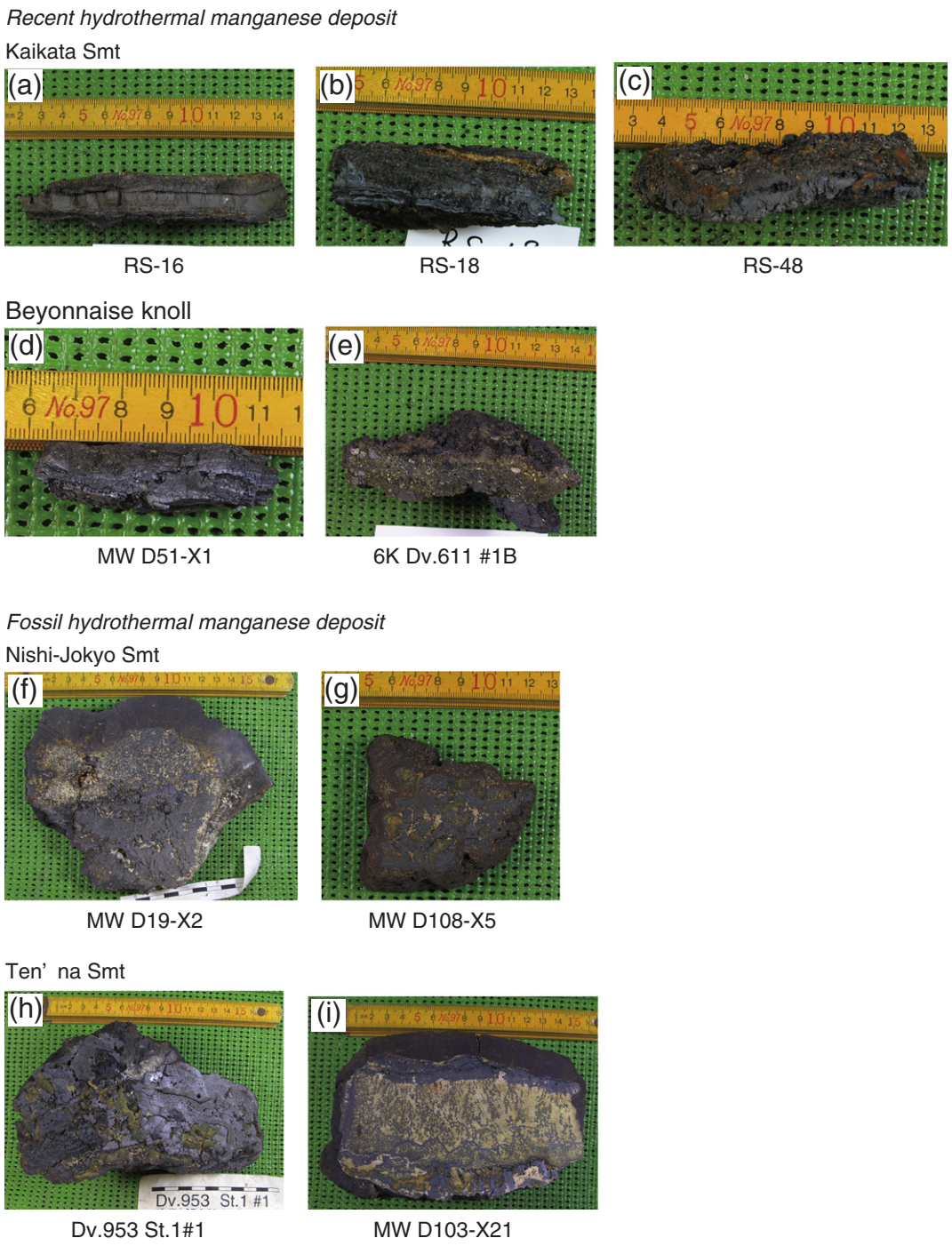

Fig. 2. Photographs of sections of hydrothermal manganese deposits from (a–c) Kaikata Smt, (d–e) Beyonnaise knoll, (f–g) Nishi–Jokyo Smt, and (h–i) Ten'na Smt. The recent hydrothermal manganese deposits are shown in in-situ orientation. Ruler shows centimeters.

black flaky manganese minerals, whereas RS-48 shows downward growing gray cusps of manganese crystals. Detailed descriptions, mineralogical information, and major chemical compositions of hydrothermal manganese deposits from the Kaikata Smt were reported by Usui et al. (1986, 1989), Usui and Nishimura (1992), and Usui and Glasby (1998).

Beyonnaise knoll, a conical caldera, hosts a large hydrothermal field associated with sulfide deposits (Hakurei site) on the southeastern margin of the caldera floor (Iizasa et al., 2004; Tanahashi et al., 2006). The knoll probably formed before or around the initiation of back-arc rifting, which occurred at ca. 2.8 Ma in the area (Iizasa et al., 2004). One sample (MW D51-X1) was dredged during the 1995 R/V *Moana Wave* cruise. Another sample (6K Dv.611#1B) was collected by the submersible *Shinkai 6500*. As presented in Fig. 2, MW D51-X1 is a 10-mm-thick, dense, laminated manganese layer overlain by a several millimeter thick layer of Mn-cemented fine volcanic sands. 6K Dv.611#1B is a 30-mm-thick coarse-grained, friable Mn oxide cemented sandstone with a dense manganese lump on the bottom.

2.2. Fossil hydrothermal manganese deposits

Fossil hydrothermal manganese deposits were collected from the Nishi-Jokyo Smt and Ten'na Smt (Fig. 1). These inactive seamounts are members of WSW–ENE trending echelon seamount chains (the Nishi-Shichito Ridge) in the back-arc region of the Izu-Ogasawara arc.

Table 2
Mineralogy and chemical composition of the hydrothermal manganese deposits.

	Recent hydrothermal manganese deposit												Fossil hydrothermal manganese deposit								Reference material	
Site	Kaikata Smt									Beyonnaise knoll			Nishi-Jokyo Smt				Ten'na Smt				C. Pacific	
Sample	RS-16			RS-18			RS-48			MW D51-X1	6K Dv.611 #1B		MW D19-X2		MW D108-X5		2K Dv.953 St.1#1		MW D103-X21		JMn-1	JMn-1[a]
Type	S	HT-1	HT-2	S	HT-1	HT-2	S	HT-1	HT-2	HT-1	S	HT-1	HG	HT-1	HG	HT-1	HG + HT	HT-1	HG	HT-1	DG	
Mineralogy (110 °C-dried samples)																						
Mn minerals	Bw	Bw	Bw	Bw	Bw	Bw	Bw	Bw	Bw	Bw		Bw	V	Bw	V	T	Bw	Bs	V	Bs	Bs	
Other minerals	pl		pl	pl	pl		pl				pl, q, sm		pl, q		pl, q				pl, q			
Chemistry (air-dried samples)																						
Na (%)	2.20	2.90	3.07	2.02	2.81	3.02	1.65	2.11	1.69	2.83	1.34	2.79	1.22	1.17	1.47	1.04	1.65	1.80	1.16	1.23	1.47	2.1
Mg	2.21	1.26	1.18	2.03	1.15	0.86	2.28	0.91	1.09	0.90	1.44	0.88	0.87	2.75	0.94	1.92	2.09	2.02	0.84	2.58	1.72	1.88
Ti	0.25	0.05	0.05	0.42	0.04	0.01	0.34	0.002	0.001	0.04	0.20	0.04	0.34	0.01	0.46	0.06	0.08	0.01	0.40	0.03	0.55	0.64
Al	4.05	0.96	0.93	7.29	0.91	0.27	6.25	0.040	0.033	0.85	3.46	0.92	0.63	0.44	2.04	0.58	0.20	0.20	1.01	0.91	1.98	2.3
Fe	3.84	0.98	2.72	6.13	0.76	1.24	5.66	0.012	0.003	0.77	14.1	0.64	16.8	0.32	15.8	2.48	6.44	0.36	16.0	0.17	8.95	10.1
Mn	20.4	36.4	32.2	7.94	37.3	38.2	12.4	40.9	41.1	37.6	0.24	34.3	15.6	39.7	7.83	39.7	35.2	42.3	14.1	42.5	22.4	25.63
Ca	4.30	2.19	2.18	5.43	2.17	2.04	6.73	1.37	1.18	1.51	2.09	1.80	1.81	1.29	1.05	0.73	1.28	1.27	1.66	1.04	1.83	2.08
K	0.57	0.37	0.25	0.43	0.39	0.19	0.29	0.11	0.12	0.43	1.53	0.33	0.31	1.04	0.52	1.03	0.93	0.92	0.39	0.80	0.62	0.78
P	0.06	0.04	0.18	0.08	0.03	0.11	0.07	0.04	0.06	0.03	0.04	0.04	0.54	0.04	0.27	0.08	0.18	0.03	0.43	0.03	0.21	0.24
Li (ppm)	296	288	28.0	111	129	1.25	94.9	1.90	1.29	312	15.1	192	3.15	350	13.5	28.9	281	473	5.43	429	57.0	71.7
Be	0.23	0.05	n.d.	0.39	0.05	n.d.	0.24	n.d.	n.d.	0.10	0.32	0.12	4.20	0.29	3.14	0.52	0.71	0.08	3.69	0.39	2.10	7.8
Sc	13.9	4.56	5.54	22.2	4.06	1.81	18.8	0.51	0.59	3.16	11.3	3.37	8.00	0.87	10.5	2.62	2.39	0.92	8.64	2.94	10.5	13
V	259	121	175	216	95.2	60.3	238	77.9	59.0	38.6	78.4	46.3	671	439	351	356	322	178	561	274	362	424
Cr	5.30	n.d.	n.d.	5.12	n.d.	n.d.	6.76	n.d.	n.d.	2.11	5.53	n.d.	16.3	n.d.	16.7	3.52	2.34	n.d.	14.7	n.d.	19.7	26.6
Co	24.1	16.1	19.8	32.2	31.4	31.8	30.4	30.6	50.1	5.18	9.59	13.3	1984	38.7	893	62.3	613	10.0	1801	58.9	1422	1732
Ni	290	14.3	17.7	97.7	16.8	n.d.	52.5	10.3	10.7	7.62	35.9	74.3	1735	901	1329	3159	2588	118	1633	3234	10,324	12,632
Cu	103	36.5	741	83.8	184	586	86.4	32.2	456	8.41	21.1	9.66	142	270	334	2427	255	22.8	188	609	8141	11,132
Zn	406	34.4	43.2	192	29.7	16.9	120	21.8	31.4	19.3	56.4	62.4	411	938	494	511	2120	83.0	399	2032	938	1068
Rb	6.27	2.48	2.02	7.00	2.14	1.13	4.11	0.58	0.68	5.34	51.7	3.30	5.15	6.07	17.8	14.0	5.39	7.57	9.43	6.93	9.48	10.9
Sr	400	380	474	381	404	450	419	367	374	290	104	347	1254	539	784	650	526	502	1142	515	682	792

(continued on next page)

Table 2 (*continued*)

	Recent hydrothermal manganese deposit												Fossil hydrothermal manganese deposit								Reference material	
Site	Kaikata Smt									Beyonnaise knoll			Nishi-Jokyo Smt				Ten'na Smt				C. Pacific	
Sample	RS-16			RS-18			RS-48			MW D51-X1	6K Dv.611 #1B		MW D19-X2		MW D108-X5		2K Dv.953 St.1#1		MW D103-X21		JMn-1	JMn-1[a]
Type	S	HT-1	HT-2	S	HT-1	HT-2	S	HT-1	HT-2	HT-1	S	HT-1	HG	HT-1	HG	HT-1	HG + HT	HT-1	HG	HT-1	DG	
Y	14.1	3.22	7.94	19.5	2.93	1.88	12.6	2.45	3.20	6.19	11.6	14.6	175	13.3	59.6	20.5	34.6	5.58	159	28.9	91.9	111
Zr	28.3	7.28	6.46	41.7	5.88	2.48	25.2	0.82	0.69	10.5	34.7	11.0	368	12.4	443	41.8	75.0	3.47	410	19.6	304	344
Nb	0.76	0.17	0.14	1.06	0.13	0.09	0.68	n.d.	n.d.	0.33	0.62	0.25	25.8	0.69	27.8	3.24	9.9	0.28	26.7	1.41	24.1	27.6
Mo	221	185	153	70.3	395	304	72.5	84.2	40.1	716	2.39	331	469	260	51.4	347	383	424	403	419	255	318
Ag	0.09	n.d.	0.02	0.12	0.02	n.d.	0.09	n.d.	n.d.	0.04	0.25	0.09	0.81	0.04	0.89	0.09	0.19	n.d.	0.85	0.05	0.66	–
Cd	10.4	1.03	0.58	2.12	2.56	0.72	2.28	0.13	0.09	2.40	0.26	2.81	3.19	63.1	2.12	9.10	36.0	31.4	2.83	104	13.1	15.5
Cs	0.25	0.05	0.05	0.25	0.04	n.d.	0.13	n.d.	n.d.	0.24	2.98	0.16	0.33	0.10	1.24	0.45	0.13	0.21	0.62	0.13	0.31	0.6
Ba	334	243	522	234	267	307	193	233	225	307	73.0	377	827	1388	1127	6623	637	1343	832	2740	1378	1714
La	4.57	0.92	1.07	5.69	0.91	0.52	3.70	0.23	0.29	2.01	2.92	1.68	253	7.19	136	31.9	33.8	1.87	234	27.0	103	122
Ce	6.95	1.65	1.48	11.8	1.39	1.12	5.86	n.d.	n.d.	3.65	7.22	2.65	727	9.25	669	53.8	108	2.56	726	3.19	227	277
Pr	1.18	0.24	0.27	1.82	0.25	0.11	1.06	0.03	0.03	0.57	1.05	0.45	53.8	1.05	27.6	6.90	7.03	0.47	51.0	6.94	25.9	31.4
Nd	6.40	1.37	1.47	9.28	1.33	0.57	5.66	0.19	0.22	2.35	5.44	2.35	247	5.02	120	33.2	32.1	1.40	225	37.2	111	137
Sm	1.83	0.39	0.46	2.67	0.35	0.16	1.66	0.04	0.04	0.54	1.55	0.62	48.5	0.96	24.8	7.43	6.98	0.32	46.5	8.63	25.3	30.2
Eu	0.62	0.18	0.23	0.99	0.17	0.09	0.62	0.06	0.06	0.23	0.50	0.30	11.7	0.55	5.86	3.07	1.80	0.35	11.0	2.86	6.42	7.6
Gd	2.19	0.50	0.65	3.39	0.42	0.22	2.06	0.11	0.14	0.77	1.99	0.88	58.7	1.57	30.2	8.20	8.60	0.42	55.2	9.49	27.8	29.8
Tb	0.35	0.08	0.10	0.57	0.08	0.03	0.33	n.d.	0.02	0.13	0.34	0.17	8.03	0.23	3.72	1.14	1.20	0.05	7.45	1.40	4.15	4.8
Dy	2.51	0.57	0.77	3.53	0.50	0.23	2.28	0.14	0.18	0.90	2.13	1.12	46.3	1.50	19.4	6.54	7.25	0.37	43.2	7.91	24.1	28.3
Ho	0.50	0.11	0.17	0.73	0.11	0.05	0.47	0.04	0.05	0.21	0.47	0.28	8.97	0.36	3.43	1.23	1.48	0.10	8.17	1.50	4.56	5.8
Er	1.66	0.34	0.59	2.31	0.33	0.17	1.47	0.16	0.18	0.63	1.39	0.89	25.7	1.2	9.69	3.33	4.38	0.34	23.9	3.97	13.2	14.6
Tm	0.22	0.05	0.08	0.33	0.05	0.02	0.20	0.02	0.03	0.10	0.21	0.14	3.51	0.17	1.30	0.43	0.63	0.05	3.18	0.54	1.85	2.1
Yb	1.51	0.35	0.60	2.21	0.32	0.17	1.40	0.16	0.23	0.64	1.37	0.92	22.8	1.17	8.76	3.07	4.09	0.33	20.8	3.36	12.3	13.8
Lu	0.23	0.05	0.08	0.33	0.05	0.02	0.20	0.03	0.03	0.11	0.21	0.17	3.34	0.21	1.27	0.44	0.65	0.06	3.03	0.48	1.79	2.1
ΣREE	30.7	6.78	8.02	45.7	6.25	3.47	27.0	1.20	1.51	12.8	26.8	12.6	1518	30.4	1061	161	218	8.70	1458	115	588	707
Ce*	0.72	0.84	0.65	0.90	0.71	1.10	0.72	–	–	0.82	1.01	0.73	1.45	0.73	2.53	0.85	1.63	0.65	1.56	0.06	1.05	
Eu*	0.95	1.25	1.28	1.01	1.38	1.52	1.02	2.73	2.03	1.11	0.87	1.22	0.67	1.35	0.65	1.20	0.71	2.87	0.66	0.96	0.74	
Ta	0.24	0.03	0.04	0.10	n.d.	0.09	0.09	n.d.	n.d.	0.04	0.08	0.03	0.30	0.04	0.40	0.06	0.08	0.09	0.34	0.04	0.60	0.64
W	5.38	20.0	18.5	4.03	25.8	15.7	4.66	23.0	29.6	23.0	0.98	6.79	65.1	77.5	10.4	72.8	66.5	66.0	56.4	60.3	34.0	45.3
Tl	12.9	0.17	0.07	2.93	1.25	0.02	2.56	n.d.	n.d.	0.27	0.66	1.98	46.2	415	6.41	15.4	306	5.40	45.4	629	161	–
Pb	9.49	2.05	1.45	12.9	1.81	0.35	6.61	n.d.	0.83	1.88	8.74	3.28	1954	24.3	1363	134	261	4.14	1624	7.71	379	430
Bi	0.10	n.d.	n.d.	0.13	0.02	n.d.	0.06	n.d.	n.d.	0.04	0.10	0.05	16.7	0.21	11.7	1.08	1.68	0.05	14.4	0.04	4.05	4.3
Th	0.38	0.07	0.06	0.49	0.05	0.02	0.31	n.d.	n.d.	0.27	0.50	0.17	35.9	0.46	35.1	3.04	6.87	0.21	36.8	0.22	10.6	11.7
U	1.01	0.72	1.04	0.41	0.43	0.19	0.41	1.71	1.47	2.93	0.22	8.33	11.8	1.01	3.85	1.20	2.09	0.39	9.84	0.42	4.44	5

Types: S = Mn-cemented sand layer, HT-1 = dense manganese layer, HT-2 = flaky manganese layer or cusps, HG = hydrogenetic manganese layer, DG = diagenetic manganese nodule.
Mineralogy: Bw = contractible buserite, Bs = resistant buserite, T = todorokite, V = vernadite, pl = plagioclase, q = quartz, sm = smectite.
Chemistry: n.d. = not detected.
Ce* and Eu* are calculated by the equations 2Ce / (La + Pr) and 2Eu / (Sm + Gd), respectively, using chondrite-normalized data.
[a] Recommended or preferable values (110 °C-dried basis) by Imai et al. (1999).

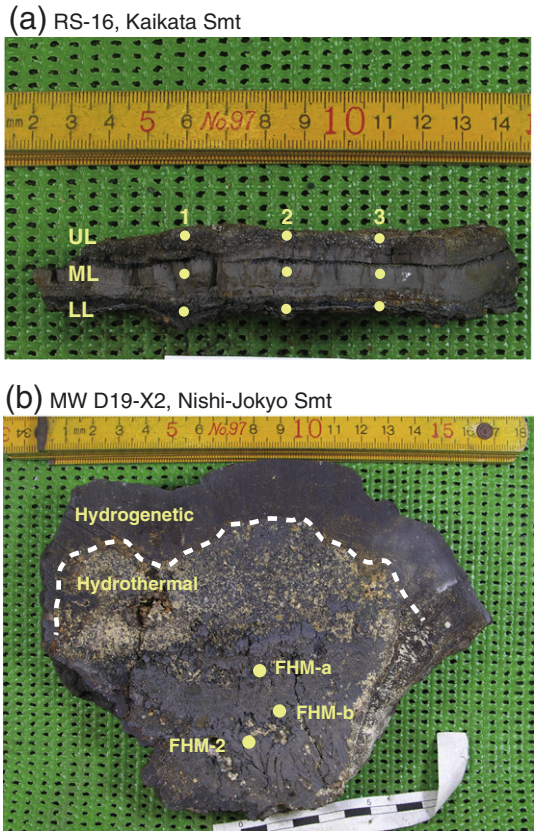

Fig. 3. (a) Photograph of the recent hydrothermal manganese deposit from the Kaikata Smt (RS-16). For U-Th age dating, three subsamples were obtained from each of the upper layer (UL), middle layer (ML), and lower layer (LL). (b) Photograph of the fossil hydrothermal manganese deposit from the Nishi-Jokyo Smt (MW D19-X2). The hydrothermal manganese deposits are overlain by a 20-mm-thick hydrogenetic manganese oxide layer. For U-Pb age dating, three subsamples were obtained from the dense submetallic manganese portion.

The Nishi-Jokyo Smt and the Ten'na Smt belong to the Enpo Chain. The Nishi-Jokyo Smt, which consists of three peaks, is located at the west end of the Empo Chain. The Ten'na Smt is conical with a flat summit located in the middle of the Enpo Chain. It is noteworthy that in the original description of the Ten'na Smt manganese crusts by Usui et al. (1986), this seamount was left unnamed, but it was previously designated as seamount D634. Many hydrothermally altered rocks and manganese deposits were collected from these seamounts with dredges and by submersible dives. The hydrothermal manganese deposits occur as massive lumps composed of Mn-cemented sandstone and layered or columnar manganese minerals with a dense, submetallic sheen (Fig. 2). The hydrothermal manganese deposits are covered with 1–20-mm-thick hydrogenetic manganese oxide layers. Two samples from the Nishi-Jokyo Smt (MW D19-X2, MW D108-X5) and one sample from the Ten'na Smt (MW D103-X21) were dredged during the 1995 R/V *Moana Wave* cruise. Sample 2K Dv.953 St.1#1 was collected from the Ten'na Smt during the *Shinkai 2000* dive in 1997. Usui and Glasby (1998) investigated another manganese sample (D634) collected from the Ten'na Smt.

3. Methods

3.1. Mineral and chemical compositions

Scanning electron microscopic (SEM) investigations were performed on the sample scratched from manganese dense layers. X-ray diffraction (XRD) analyses were conducted on the powdered sample analyzed for chemical composition at Kochi University, with Cu Kα

Table 3
Correlation coefficient matrix for compositional data of the recent and fossil hydrothermal manganese deposits.

	Na	Mg	Ti	Al	Fe	Mn	Ca	Li	Sc	V	Cr	Co	Ni	Cu	Zn	Sr	Y	Mo	Cd	Ba	ΣREE	Pb	U
Na	1.00	−0.72	−0.16	−0.12	−0.30	0.13	0.08	−0.14	−0.06	−0.65	−0.28	−0.22	−0.60	−0.32	−0.52	−0.27	−0.55	0.19	−0.53	−0.53	−0.54	−0.37	0.27
Mg		1.00	0.36	0.34	0.17	−0.17	0.25	0.53	0.31	0.89	0.50	0.23	0.53	0.12	0.64	0.48	0.65	−0.02	0.70	0.36	0.49	0.28	−0.37
Ti			1.00	0.99	0.64	−0.88	0.90	−0.15	0.99	0.18	0.82	−0.04	−0.19	−0.20	−0.10	−0.27	0.28	−0.44	−0.24	−0.20	0.04	−0.05	−0.22
Al				1.00	0.58	−0.87	0.92	−0.14	0.99	0.13	0.84	−0.18	−0.26	−0.24	−0.17	−0.31	0.19	−0.45	−0.22	−0.23	−0.08	−0.21	−0.22
Fe					1.00	−0.87	0.38	−0.29	0.61	0.07	0.46	0.23	−0.03	−0.11	0.04	−0.49	0.32	−0.43	−0.21	−0.15	0.23	0.24	−0.22
Mn						1.00	−0.73	0.30	−0.89	0.02	−0.83	0.10	0.32	0.28	0.21	0.57	−0.15	0.55	0.33	0.32	0.08	0.13	0.18
Ca							1.00	−0.16	0.92	0.06	0.80	−0.17	−0.38	−0.32	−0.25	−0.21	0.02	−0.42	−0.31	−0.37	−0.21	−0.25	−0.20
Li								1.00	−0.17	0.36	−0.52	0.14	0.24	−0.29	0.48	0.26	0.32	0.59	0.67	0.06	0.18	0.04	0.05
Sc									1.00	0.11	0.84	−0.15	−0.27	−0.23	−0.17	−0.31	0.19	−0.45	−0.27	−0.25	−0.07	−0.18	−0.23
V										1.00	0.00	0.36	0.65	0.41	0.65	0.70	0.66	0.03	0.60	0.55	0.63	0.51	−0.28
Cr											1.00	−0.51	−0.52	−0.24	−0.51	−0.29	−0.33	−0.87	−0.53	−0.27	−0.54	−0.58	−0.90
Co												1.00	0.51	0.04	0.70	0.30	0.65	0.16	0.23	0.03	0.78	0.91	0.06
Ni													1.00	0.66	0.83	0.65	0.80	0.33	0.66	0.77	0.90	0.67	−0.09
Cu														1.00	0.17	0.63	0.26	0.10	0.08	0.90	0.50	0.37	−0.13
Zn															1.00	0.48	0.86	0.28	0.82	0.33	0.82	0.65	−0.06
Sr																1.00	0.37	0.29	0.46	0.66	0.52	0.45	−0.14
Y																	1.00	0.15	0.58	0.40	0.88	0.70	0.10
Mo																		1.00	0.32	0.27	0.24	0.18	0.26
Cd																			1.00	0.34	0.45	0.17	−0.14
Ba																				1.00	0.59	0.38	−0.08
ΣREE																					1.00	0.90	−0.02
Pb																						1.00	0.06
U																							1.00

The values |X| ≥ 0.8 are underlined.

radiation at 40 kV and 16 mA. Before XRD analysis, the sample was dried at 110 °C for 3 h because buserite is indistinguishable from todorokite in an air-dried sample.

Samples for chemical analyses were scraped with a ceramic knife. For recent hydrothermal manganese deposits, samples were collected from each layer showing different structures. For fossil hydrothermal manganese deposits, samples were collected from dense submetallic parts. Surface 3 mm of hydrogenetic manganese layers were also collected. For chemical analyses, approximately 20 mg of the powdered sample was weighed in a Teflon vial and was completely digested using a HCl-HF acid mixture. After the sample was dried, the residue was dissolved in dilute HNO_3 and then analyzed at the Geological Society of Japan. Major elements (Na, Mg, Ti, Al, Fe, Mn, Ca, K, P) were determined using inductively coupled plasma–atomic emission spectrometry (ICP-AES, SPS7800; Seiko Instruments Inc.). Minor elements were determined using inductively coupled plasma–mass spectrometry (ICP-MS, 7700x; Agilent) combined with the indium internal standard technique. To assess the analytical precision and accuracy, the GSJ geochemical reference material JMn-1 (manganese nodule, air-dried) was regularly measured (RSD $< \pm 5\%$, $n = 24$). The obtained element concentrations of JMn-1 are presented in Table 2. It is noteworthy that the certified values (Imai et al., 1999) are based on analyses of a 110 °C-dried sample. Because of the considerable water content of JMn-1, the obtained concentrations are about 20% lower than the certified values. The total procedural blanks were also checked to ensure negligible effects.

3.2. U-Th and U-Pb age dating

A recent hydrothermal manganese deposit from the Kaikata Smt (RS-16) was used for U-Th dating. Three subsamples (100–200 mg) each were collected by drilling from the upper Mn-cemented sand layer, the middle gray dense layer, and the bottom black laminated layer (Fig. 3a). The fossil hydrothermal manganese deposit from the Nishi-Jokyo Smt (MW D19-X2) was used for U-Pb dating. Three subsamples (ca. 500 mg) were collected from the dense submetallic manganese part. The detritus was eliminated carefully (Fig. 3b). These samples were homogenized using an agate mortar.

Isotopic compositions of U, Th, and Pb were determined at The University of Texas at El Paso using techniques described by Granet et al. (2007), Pelt et al. (2008), and Konter and Jackson (2012). For measurements of U and Th isotopic compositions and concentrations, 70–100 mg powdered samples were weighed in a Teflon vial and were spiked with mixed ^{233}U-^{229}Th. For Pb analysis, two aliquots of 25 mg powdered samples were weighed in Teflon vials: one aliquot was ^{206}Pb-spiked for Pb concentration measurements; the other unspiked aliquot was for Pb isotope compositions. The samples were dissolved completely using a HCl-HF acid mixture. Anion-exchange chromatography was used for U, Th, and Pb separation and purification. The total procedural blanks are ~6 pg for U, ~40 pg for Th, and ~25 pg for Pb, which have negligible amounts of U, Th, and Pb in the samples.

Isotope measurements were performed using a Nu Instruments Nu Plasma MC-ICP-MS. A sample-standard bracketing method was used to correct for instrumental mass bias. A Tl doping technique was used for Pb isotope analyses. U concentrations were calculated using the measured $^{235}U/^{233}U$ isotopic ratios. ($^{234}U/^{238}U$) activity ratios were calculated using the analyzed $^{234}U/^{235}U$ ratios and by assuming a constant $^{238}U/^{235}U$ ratio of 137.88, with the following decay constants: $\lambda_{238} = 1.551 \times 10^{-10}$ yr^{-1} and $\lambda_{234} = 2.826 \times 10^{-6}$ yr^{-1} (Akovali, 1994; Cheng et al., 2000). Duplicate analyses of basalt BCR-2 rock standard yielded a mean ($^{234}U/^{238}U$) activity ratio of 1.003 ± 0.002, a mean U concentration of 1.684 ± 0.004 ppm, a mean ($^{230}Th/^{232}Th$) activity ratio of 0.877 ± 0.005, and a mean Th concentration of 5.807 ± 0.012. The obtained $^{206}Pb/^{204}Pb$, $^{207}Pb/^{204}Pb$, $^{208}Pb/^{204}Pb$ ratios and Pb concentration of BCR-2 were, respectively, 18.761, 15.618, 38.750, and 10.60 ppm. These values are consistent with previously published values (e.g., Baker et al., 2004; Matthews et al., 2011). Closed-system U-series ages and parameters of isochrones were calculated using the ISOPLOT program (Ludwig, 2012).

4. Results and discussion

Mineralogy and chemical composition are presented in Table 2.

4.1. Mineralogy

SEM images showed a honeycomb structure of blade-shaped crystals for the recent and fossil hydrothermal manganese deposits from all sites. The manganate crystals are several hundred micrometers long and several micrometers thick, making them much larger than those found in hydrogenetic or diagenetic manganese deposits. These mineralogical characteristics are typical in hydrothermal manganese

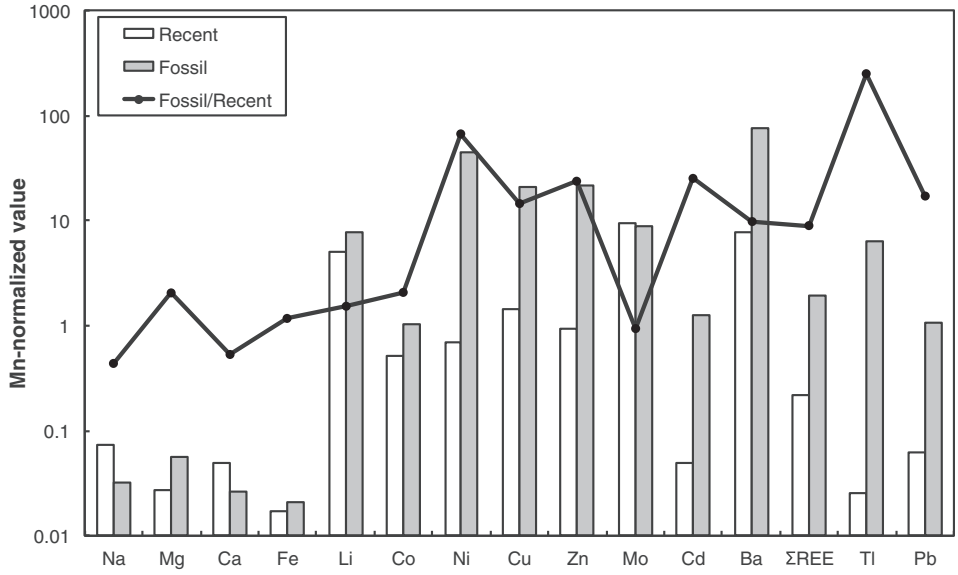

Fig. 4. Selected element concentrations of dense manganese layers from the recent (white bar) and fossil (gray bar) hydrothermal manganese deposits. All data are normalized with respect to Mn concentrations. Na, Mg, Ca, and Fe are expressed as %/%; the others are as ppm/%. The solid line represents the ratio of Mn-normalized element concentration in fossil samples to that in recent samples.

deposits from the Kaikata Smt (Usui et al., 1989) and the Ten'na Smt (Usui and Glasby, 1998).

Recent hydrothermal manganese deposits consist mainly of collapsible birnessite (7 Å manganate). Compared to the uppermost Mn-cemented sand layer, the dense manganese layers contain less silicate minerals (plagioclase, quartz, smectite). For the fossil hydrothermal manganese deposits, collapsible birnessite and todorokite (10 Å manganate) were detected from the Nishi-Jokyo Smt samples. In the case of the Ten'na Smt, the hydrothermal manganates consist of stable birnessite (7 Å + 10 Å manganate). The surface hydrogenetic manganese layers comprise vernadite along with minor quartz and plagioclase, except for a very thin black layer of 2K Dv.953 St.1#1 (Ten'na Smt) showing collapsible birnessite. This thin layer is likely a mixture of hydrogenetic and hydrothermal origin. Based on the spacial distribution of Mn minerals in hydrothermal manganese deposits from the Kaikata Smt, Usui et al. (1989) proposed that higher temperatures of mineralization produced more stable 10 Å phases, with closer proximity to the hydrothermal source. The higher 10 Å stability in the fossil manganese deposits suggests that they formed from higher temperature mineralizing fluids than the recent samples did. Another possibility for the increase in 10 Å stability is the uptake of stabilizing interlayer cations as discussed in detail below.

4.2. Chemical composition

The recent hydrothermal manganese deposits have 32–41% Mn, except for the Mn-cemented sand layers (0.2–20% Mn). The Mn-cemented sand layers show higher aluminosilicate-associated elements (Ti, Al, Ca,

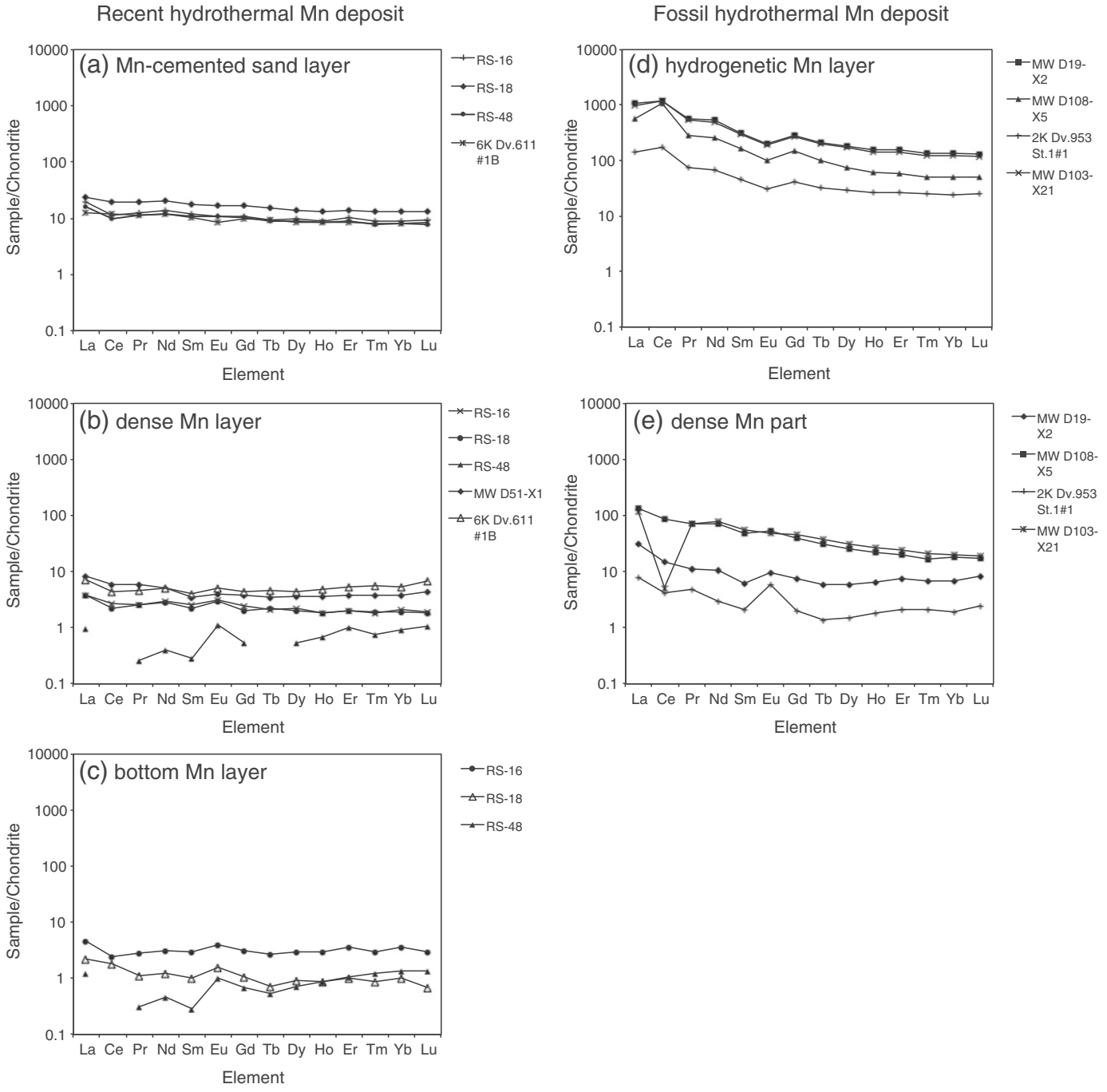

Fig. 5. Rare earth element (REE) patterns normalized to chondrites (Sun and McDonough, 1989) for the recent and fossil hydrothermal manganese deposits in the Izu-Ogasawara arc.

Sc, and Cr). These elements positively correlate mutually and correlate negatively with Mn, indicating their association with detrital materials (Table 3). Fe/Mn ratios for the Mn-cemented sandstone samples are 0.2–59, whereas those for the stratabound Mn samples are significantly low (0.0001–0.08). Fe, V, Ni, Zn, Rb, Y, Zr, REE, Tl, and Pb also showed higher concentration in the Mn-cemented sandstone. However, the stratabound Mn is more enriched in Mn, Mo, W, and U. Among the hydrothermal manganese deposits from Kaikata Smt, the middle and bottom manganese layers basically showed similar chemical compositions. However, the bottom surface layers were clearly depleted in Li, and were significantly enriched in Cu compared to the middle layers. Compared to hydrogenetic ferromanganese crusts, the mean concentrations for Fe (0.9%), Co (25 ppm), Ni (22 ppm), Cu (257 ppm), Zn (32 ppm), REE (0.06–2 ppm), and Pb (1.7 ppm) of the stratabound Mn were 1–2 orders of magnitude smaller. By contrast, the mean concentration for Li (119 ppm) is much higher. These characteristics are typical of materials with a hydrothermal origin (e.g., Glasby et al., 1997; Hein et al., 2008; Usui and Someya, 1997). High Mg, Co, Mo, Cd, and Ba contents have been reported for other hydrothermal manganese deposits, suggesting the hydrothermal contributions of these elements (e.g., Hein et al., 2008; Kuhn et al., 2003; Moorby et al., 1984; Usui and Someya, 1997). However, the recent hydrothermal manganese deposits analyzed here showed no prominent enrichment for these elements.

The chemical compositions of the fossil hydrothermal manganese deposits resemble those of recent deposits, but most heavy metal elements are more abundant in the fossil deposits. Ni, Cu, Zn, Cd, Ba, REE, Tl, and Pb are particularly enriched, more than tenfold in the fossil deposits relative to the dense Mn layers of the recent deposits. Fig. 4 shows Mn-normalized values of selected elements in the recent and fossil hydrothermal manganese deposits. In contrast to these elements, Li, Co, and Mo exhibit no significant differences, implying similar levels of hydrothermal contributions, which suggests that Ni, Cu, Zn, Cd, Ba, REE, Tl, and Pb contents have increased selectively after formation of the deposits. Buserite is known to take up cations such as Ni^{2+}, Cu^{2+}, and Ba^{2+} strongly into 10 Å manganate interlayers. Considering the decreases in Na and Ca abundances for the fossil deposits, these elements might concentrate by ion exchange with Na and Ca. Based on a comparison of older and younger hydrothermal manganese deposits from the Galapagos spreading centre, Clauer et al. (1984) reported increases in Cu + Ni + Co contents and extensive exchange of REE with age. Nedjatpoor et al. (1985) showed increasing occurrence of 10 Å manganate with age in diagenetic nodules in the Peru Basin. Structural stabilization by cation uptake might explain the more abundant 10 Å manganate in the fossil hydrothermal manganese deposits, although higher temperatures of mineralization cannot be ruled out.

Chondrite-normalized REE patterns of the recent manganese samples (Figs. 5a–5c) showed negative Ce anomalies and positive Eu anomalies, although the anomalies were small. The Mn-cemented sand layers show no distinct anomalies attributable to the incorporation of detrital materials. The average values of Ce* and Eu* in the recent manganese samples are, respectively, 0.82 and 1.36 (Table 2). These anomalies contrast to those in the hydrogenetic manganese layer, which shows positive Ce anomalies and negative Eu anomalies (Fig. 5d). Negative Ce anomalies have been reported from many other hydrothermal manganese deposits, reflecting rapid precipitation of the manganese minerals (Bau et al., 2014; Hein et al., 2008; Hodkinson et al., 1994). Positive Eu anomalies are not common in hydrothermal manganese deposits, but they have been reported from the Izu-Ogasawara arc (Usui and Glasby, 1998). The positive Eu anomalies suggest that the end-member hydrothermal fluids had temperatures >200–250 °C (Bau, 1991; Glasby et al., 1997). The fossil hydrothermal manganese deposits show similar REE patterns, but the Ce and Eu anomalies are more prominent. Their average values of Ce* and Eu* are, respectively, 0.57 and 1.60 (Table 2). Moreover, light REE was more enriched than those of the recent hydrothermal manganese deposits (Fig. 5e). This trend indicates that light REEs were increasingly scavenged from ambient seawater or porewater after deposition. Such aging effects have demonstrated an increase in the magnitude of the negative Ce anomaly in hydrothermal manganese deposits (Bau et al., 2014), but in our deposits, the Ce anomaly remained small, except for one sample.

4.3. U-Th age of recent hydrothermal manganese deposits

The hydrothermal manganese deposits include some detrital ^{230}Th and ^{234}U. Therefore, the initial ^{230}Th and ^{234}U must be subtracted respectively from the total measured ^{230}Th and ^{234}U before U-Th age calculations are made. In Fig. 6, detritus-corrected $^{230}Th/^{238}U$ versus $^{234}U/^{238}U$ ratios are obtained by extrapolation of ^{232}Th to 0 because ^{232}Th is generally of detrital origin. The good linearity depicted in Fig. 6 demonstrates that the sample is a two-component mixture of an isotopically homogeneous detrital material with a pure Mn oxide.

Assuming a closed system for U, the upper layer (Mn-cemented sand layer) showed a $^{230}Th/^{234}U$ age of 8.8 ± 0.94 ka (MSWD = 0.35, probability = 0.71) based on the calculation using ISOPLOT (Fig. 7). The estimated initial $^{234}U/^{238}U$ activity ratio was 1.150 ± 0.007, which is consistent with the average value of seawater (1.1466–1.1496; Andersen et al., 2010; Delanghe et al., 2002; Robinson et al., 2004). This fact suggests that the uranium in this deposit was incorporated from seawater. On the other hand, the middle and lower layers do not show good $^{230}Th/^{234}U$ ages because of the small variations in Th/U ratios (Fig. 6). The low Th/U ratios indicate that they contain almost no detrital materials. Nevertheless, it is suggested that the middle layer is younger than the upper layer and the lower is younger than the middle layer

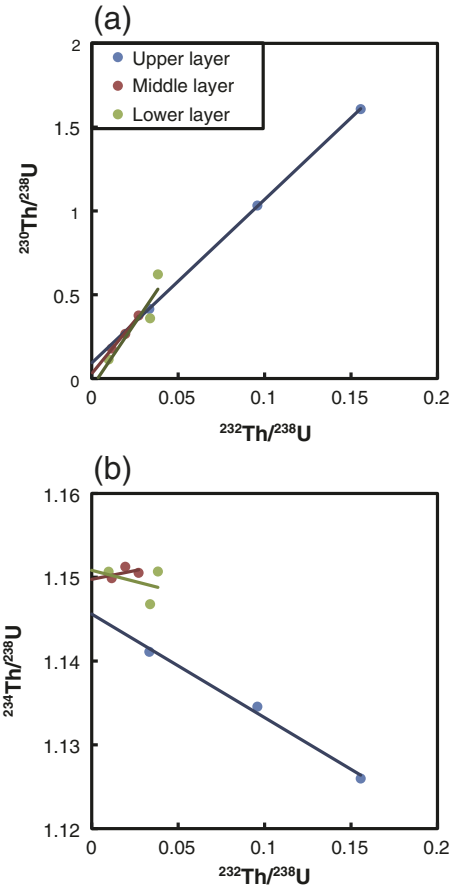

Fig. 6. Diagrams of (a) $^{232}Th/^{238}U$-$^{230}Th/^{238}U$ and (b) $^{232}Th/^{238}U$–$^{234}U/^{238}U$ for the recent hydrothermal manganese deposit from the Kaikata Smt (RS-16). Blue, red, and green circles respectively represent upper, middle, and lower layers. Color lines show linear regressions for data points of the same color. ^{232}Th = 0 gives detritus-corrected $^{230}Th/^{238}U$ and $^{234}U/^{238}U$.

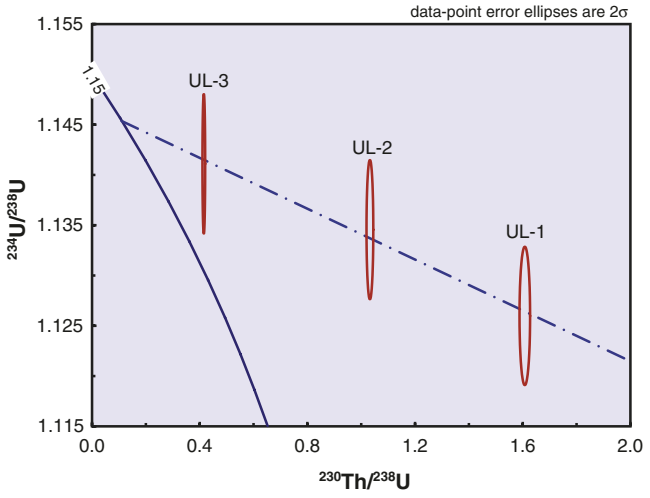

Fig. 7. ^{234}U-^{230}Th isochron for the upper layer of the recent hydrothermal manganese deposit from the Kaikata Smt (RS-16). $^{230}Th/^{234}U$ age was calculated using Isoplot 4.16 (Ludwig, 2012).

based on the inferred $^{230}Th/^{238}U$ of the pure Mn oxides (Fig. 6). Holocene formation of these layers is also supported by the fact that the measured $^{234}U/^{238}U$ activity ratios do not deviate from the seawater value of 1.15 (Table 4). Reports of several studies have suggested that hydrothermal manganese deposits do not remain a closed system with respect to uranium (Hodkinson et al., 1994; Moore and Vogt, 1976). The uniform U concentrations (approx. 1 ppm) and $^{234}U/^{238}U$ activity ratios close to the seawater value in this study, however, imply little effect on age calculations. Some $^{230}Th/^{234}U$ ages of hydrothermal manganese deposits from mid-ocean ridges, island arcs, and hot spot volcanoes are available for comparison (Cronan et al., 1982; Hodkinson et al., 1994; Moore and Vogt, 1976; Scott et al., 1974). However, these ages were determined using single-point measurement from each layer and ^{230}Th that originated from detrital material was not corrected. This has presented a severe problem for age estimation, especially for the Mn-cemented sand layer, as pointed out by Burnett and Piper (1977). This study demonstrates that detritus correction by multipoint measurement was useful to obtain a more reliable U-Th age.

The $^{230}Th/^{234}U$ age of the upper layer yields an average growth rate of ca. 2 mm/kyr for the 20-mm-thick hydrothermal manganese deposit if the lower layer formed very recently. This value is approximately three orders of magnitude faster than that of hydrogenetic Mn crusts. Alternatively, growth rates might be calculated using the empirical equation of Manheim and Lane-Bostwick (1988): growth rate (mm/Myr) $R = 0.68/(Co^n)^{1.67}$, where the normalized Co is $Co^n = Co \times 50/(Fe + Mn)$, and Co, Fe, and Mn are concentrations measured in weight percent. According to the equation, the upper layer has a growth rate of 4.8 mm/kyr, although the middle and lower layers have faster growth rates (12–19 mm/kyr). Growth rates of 0.1–2 mm/kyr have been estimated for other hydrothermal manganese deposits using U-Th age dating (Cronan et al., 1982; Hodkinson et al., 1994; Moore and Vogt, 1976; Scott et al., 1974). However, the growth rates based on the Co content showed a wide range of 0.2 to >200 mm/kyr (Hein et al., 1990; Hein et al., 2008; Sun et al., 2011). Different growth rates of each layer are likely caused by the episodic accumulations of manganese oxides. However, it is noteworthy that temporal variations in Co concentration of hydrothermal fluids vary the Co distribution in hydrothermal manganese deposits.

Based on textural data (orientation of columnar, botryoidal, and scalloped structures) and in situ submersible observation, Usui and Nishimura (1992) proposed a model for the formation of the hydrothermal manganese deposits from the Kaikata Smt. After deposition of volcanic sands, the discharged low-temperature hydrothermal fluids precipitated manganese oxides at the sediment–water interface and cemented the surface sand layers as hardpan, acting like a cap on the ascending fluids. Subsequently, pure and dense manganese layers developed beneath the cemented surface. The discharge of hydrothermal fluids was probably intermittent. The individual layers were formed from multiple episodes of precipitation. A similar model has been described by Schulz and Hein (1991) for the Mariana arc, Hein et al. (1990) for Tonga Ridge, and Hodkinson et al. (1994) for the Pitcairn Island hotspot. This model is supported strongly by the absolute ages in this study.

4.4. U-Pb age of fossil hydrothermal manganese deposits

The lead isotopic compositions of hydrothermal manganese oxides from sample MW D19-X2 showed $^{206}Pb/^{204}Pb = 18.570–18.577$ and $^{207}Pb/^{204}Pb = 15.641–15.643$ (Table 5), which are in agreement with data for the hydrogenetic Mn crusts from the Izu-Ogasawara back-arc region ($^{206}Pb/^{204}Pb = 18.54–18.59$ and $^{207}Pb/^{204}Pb = 15.64–15.66$; Chu et al., 2006). These values are less radiogenic than hydrogenetic manganese crust from the central North Pacific (Ling et al., 2005), but significantly higher than the Izu-Ogasawara arc rocks. Ling et al. (2005) concluded that lead in hydrogenetic manganese crusts recorded the dissolved lead in seawater derived mainly from eolian dust. The less radiogenic lead isotopic ratios observed in the Izu-Ogasawara area suggest some contribution of mantle-derived lead to seawater. It is noteworthy that the hydrothermal and hydrogenetic manganese oxides showed consistent lead isotopic ratios in the Izu-Ogasawara area. These consistent ratios suggest that lead was mainly incorporated from interstitial seawater rather than hydrothermal fluids in the analyzed hydrothermal manganese samples.

The initial $^{206}Pb/^{204}Pb$ ratio of 18.5689 ± 0.0018 was estimated using the $^{238}U/^{204}Pb$-$^{206}Pb/^{204}Pb$ isochron (Fig. 8). Based on calculations using ISOPLOT, the $^{206}Pb/^{238}U$ age of the fossil hydrothermal manganese oxides from the Nishi-Jokyo Smt showed 4.4 ± 1.6 Ma (MSWD = 1.8). The uniform U concentrations (approx. 1 ppm) and $^{234}U/^{238}U$ activity ratios (0.93–1.0) imply that this deposit has remained a closed system for uranium. If the hydrogenetic manganese precipitation started soon after formation of the hydrothermal deposit, a growth rate of 4.5 mm/

Table 4
U-series data for RS-16 from the Kaikata Smt.

Sample	^{238}U (ppm)	^{232}Th (ppm)	$(^{230}Th/^{238}U) \pm 2\sigma$	$(^{234}U/^{238}U) \pm 2\sigma$	$(^{232}Th/^{238}U) \pm 2\sigma$
UL-1	1.007	0.479	1.608 ± 0.016	1.126 ± 0.006	0.156 ± 0.0019
UL-2	1.044	0.306	1.032 ± 0.010	1.135 ± 0.006	0.096 ± 0.0011
UL-3	1.562	0.159	0.415 ± 0.004	1.141 ± 0.006	0.033 ± 0.0004
ML-1	0.919	0.032	0.179 ± 0.002	1.150 ± 0.006	0.012 ± 0.0001
ML-2	0.998	0.083	0.376 ± 0.004	1.151 ± 0.006	0.027 ± 0.0003
ML-3	0.954	0.057	0.266 ± 0.003	1.151 ± 0.006	0.019 ± 0.0002
LL-1	1.094	0.113	0.359 ± 0.004	1.147 ± 0.006	0.034 ± 0.0004
LL-2	1.214	0.036	0.114 ± 0.001	1.151 ± 0.006	0.010 ± 0.0001
LL-3	1.431	0.167	0.621 ± 0.006	1.151 ± 0.006	0.038 ± 0.0005

U and Th concentrations were calculated using the measured $^{235}U/^{233}U$ and $^{232}Th/^{229}Th$ isotopic ratios, respectively. $(^{234}U/^{238}U)$ activity ratios were calculated using the analyzed $^{234}U/^{235}U$ ratios and assuming a constant $^{238}U/^{235}U$ ratio of 137.88, with the following decay constants: $\lambda_{238} = 1.551 \times 10^{-10}$ yr^{-1} and $\lambda_{234} = 2.826 \times 10^{-6}$ yr^{-1} (Akovali, 1994; Cheng et al., 2000). Parenthesis means activity ratios hereafter.

Table 5
U and Pb data for MW D19-X2 from the Nishi-Jokyo Smt.

Sample	U (ppm)	Pb (ppm)	$^{206}Pb/^{204}Pb$	$^{207}Pb/^{204}Pb$	$^{208}Pb/^{204}Pb$	$^{238}U/^{204}Pb \pm 2\sigma$	$^{235}U/^{204}Pb \pm 2\sigma$	$(^{234}U/^{238}U)$
FHM-2	1.041	23.92	18.570	15.643	38.818	2.804 ± 0.028	0.020 ± 0.0002	0.966
FHM-a	1.015	18.57	18.572	15.643	38.816	3.522 ± 0.035	0.026 ± 0.0003	1.002
FHM-b	0.985	5.196	18.577	15.641	38.816	12.21 ± 0.122	0.089 ± 0.0009	0.925

Errors of $^{206}Pb/^{204}Pb$, $^{207}Pb/^{204}Pb$, and $^{208}Pb/^{204}Pb$ are ±0.001, ±0.001, ±0.002, respectively (2σ).

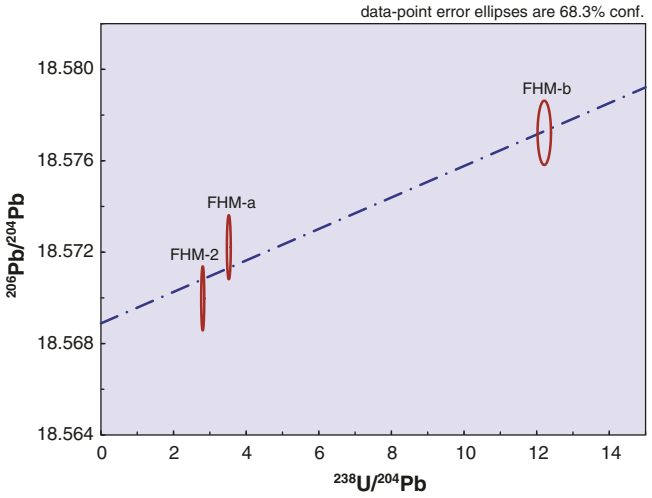

Fig. 8. ^{238}U-^{206}Pb isochron for the fossil hydrothermal manganese deposit from the Nishi-Jokyo Smt (MW D19-X2). $^{206}Pb/^{238}U$ age was calculated using Isoplot 4.16 (Ludwig, 2012).

Myr would be required to form the 20 mm-thick hydrogenetic manganese crust that overlies the hydrothermal oxides, which is within the growth rate range of most crusts.

Hydrothermal mineralization of manganese in the back-arc region of the Izu-Ogasawara arc would have occurred in association with volcanism. The hydrothermal manganese deposits from the Ten'na Smt contained many Quaternary foraminifera tests, showing that formation of the manganese deposit started sometime later during the Quaternary (Usui et al., 1986). U-Th dating showed an age of ca. 0.5 Ma (unpublished data from Usui and Glasby, 1998). Based on the foraminifera age of limestone bedrock and the thickness of the overlying hydrogenetic manganese layer, the hydrothermal manganese deposits at the Tenpo Smt formed after the Miocene (Usui and Nishimura, 1993).

This report is the first study that directly determines the age of fossil hydrothermal manganese deposits, although very young hydrothermal manganese deposits have been dated radiometrically. The results provide information related to the volcanism and hydrothermal activity associated with formation of manganese deposits. $^{40}Ar/^{39}Ar$ age dating for the dredged volcanic rocks from the Nishi-Jokyo Smt revealed that the andesite erupted at 10.7 ± 0.2 Ma, and that of basalt is 5.8 ± 0.3 Ma (Ishizuka et al., 1998). The obtained age for the hydrothermal manganese deposit (4.4 ± 1.6 Ma) is contemporary with the basaltic volcanism (5.8 ± 0.3 Ma). That age suggests that the hydrothermal Mn deposit was formed by hydrothermal activity related to the basaltic volcanism. The age of the fossil hydrothermal manganese deposit also provides a vector to explore for fossil sulfide deposits because manganese mineralization often occurs around sulfide deposits in modern hydrothermal systems. Sulfide minerals precipitate from high temperature hydrothermal fluids, whereas manganese oxides precipitate from diffuse low temperature hydrothermal fluids.

5. Conclusions

The mineralogy and chemical compositions of hydrothermal manganese deposits in the Izu-Ogasawara arc are of typical hydrothermal origin. Comparison of recent and fossil samples, however, demonstrated that the fossil hydrothermal manganese deposits had higher contents of Ni, Cu, Zn, Cd, Ba, REE, Tl, and Pb, and more enrichment in light REEs. It is suggested that these metals increased with age by post-depositional scavenging from seawater. This study also presents reliable U-Th and U-Pb ages of hydrothermal manganese deposits by using a technique that corrects for detritus. The U-Th ages of the Holocene deposit from the Kaikata Smt showed 8.8 ± 0.94 ka for the uppermost layer, which is the oldest layer, and downward mineral precipitation with a rapid growth rate of ca. 2 mm/kyr; this is consistent with the proposed model for the formation of hydrothermal manganese deposits based mainly on textural observation. The U-Pb age of the fossil deposit from the Nishi-Jokyo Smt is 4.4 ± 1.6 Ma, suggesting that the deposit formed during hydrothermal activity associated with the basaltic volcanism at 5.8 ± 0.3 Ma. Although hydrothermal manganese deposits seem economically less important because of their low contents of valuable trace metals, their age can be an indicator to facilitate exploration for polymetallic sulfide deposits. Moreover, Mn itself is an economically valuable metal.

Acknowledgements

We appreciate the useful comments offered by two anonymous reviewers and the Guest Editor, Dr. James R. Hein. This study was supported by JSPS KAKENHI Grant Numbers JP15K17790 and JP23540535.

References

Akovali, Y.A., 1994. Nuclear data sheets for A = 234. Nucl. Data Sheets 71, 18.
Andersen, M.B., Stirling, C.H., Zimmermann, B., Halliday, A.N., 2010. Precise determination of the open ocean $^{234}U/^{238}U$ composition. Geochem. Geophys. Geosyst. 11, Q12003. http://dx.doi.org/10.1029/2010GC003318.
Baker, J., Peate, D., Waight, T., Meyzen, C., 2004. Pb isotopic analysis of standards and samples using a ^{207}Pb–^{204}Pb double spike and thallium to correct for mass bias with a double-focusing MC-ICP-MS. Chem. Geol. 211, 275–303.
Bau, M., 1991. Rare-earth element mobility during hydrothermal and metamorphic fluid–rock interaction and the significance of the oxidation state of europium. Chem. Geol. 93, 219–230.
Bau, M., Schmidt, K., Koschinsky, A., Hein, J., Kuhn, T., Usui, A., 2014. Discriminating between different genetic types of marine ferro-manganese crusts and nodules based on rare earth elements and yttrium. Chem. Geol. 381, 1–9.
Burnett, W.C., Piper, D.Z., 1977. Rapidly formed ferromanganese deposit from the eastern Pacific Hess Deep. Nature 265, 596–600.
Cheng, H., Edwards, R.L., Hoff, J., Gallup, C.D., Richards, D.A., Asmerom, Y., 2000. The half-lives of uranium-234 and thorium-230. Chem. Geol. 169, 17–33.
Chu, N.-C., Johnson, C.M., Beard, B.L., German, C.R., Nesbitt, R.W., Frank, M., Bohn, M., Kubik, P.W., Usui, A., Graham, I., 2006. Evidence for hydrothermal venting in Fe isotope compositions of the deep Pacific Ocean through time. Earth Planet. Sci. Lett. 245, 202–217.
Clauer, N., Stille, P., Bonnot-Courtois, C., Moore, W.S., 1984. Nd-Sr isotopic and REE constraints on the genesis of hydrothermal manganese crusts in the Galapagos. Nature 311, 743–745.
Cronan, D.S., Glasby, G.P., Moorby, S.A., Thomson, J., Knedler, K.E., McDougall, J.C., 1982. A submarine hydrothermal manganese deposit from the south-west Pacific island arc. Nature 298, 456–458.
Delanghe, D., Bard, E., Hemelin, B., 2002. New TIMS constrains on the uranium-238 and uranium-234 in seawaters from the main ocean basins and the Mediterranean Sea. Mar. Chem. 80, 79–93.
Glasby, G.P., Stüben, D., Jeschke, G., Stoffers, P., Garbe-Schönberg, C.D., 1997. A model for the formation of hydrothermal manganese crusts from the Pitcairn Island hotspot. Geochim. Cosmochim. Acta 61, 4583–4597.
Granet, M., Chabaux, F., Stille, P., France-Lanord, C., Pelt, E., 2007. Time-scales of sedimentary transfer and weathering processes from U-series nuclides: clues from the Himalayan rivers. Earth Planet. Sci. Lett. 261, 389–406.

Hein, J.R., 2004. Cobalt-rich ferromanganese crusts: global distribution, composition, origin and research activities. Workshop on Minerals Other than Polymetallic Nodules of the International Seabed Area vol. 1. Int. Seabed Auth, Kingston, pp. 188–256.
Hein, J.R., Schultz, M.S., Kang, J.-K., 1990. Insular and submarine ferromanganese mineralization of the Tonga-Lau region. Mar. Min. 9, 305–354.
Hein, J.R., Koschinsky, A., Halbach, P., Manheim, F.T., Bau, M., Kang, J.-K., Lubick, N., Nicholson, K., Hein, J.R., Bühn, B., Dasgupta, S., 1997. Iron and manganese oxide mineralization in the Pacific. Manganese Mineralization: Geochemistry and Mineralogy of Terrestrial and Marine Deposits. Geological Society of London Special Publication No. 119, London, pp. 123–138.
Hein, J.R., Schulz, M.S., Dunham, R.E., Stern, R.J., Bloomer, S.H., 2008. Diffuse flow hydrothermal manganese mineralization along the active Mariana and southern Izu-Bonin arc system, western Pacific. J. Geophys. Res. 113, B08S14. http://dx.doi.org/10.1029/2007JB005432.
Hodkinson, R.A., Stoffers, P., Scholten, J., Cronan, D.S., Jeschke, G., Rogers, T.D.S., 1994. Geochemistry of hydrothermal manganese deposits from the Pitcairn Island hotspot, southeastern Pacific. Geochim. Cosmochim. Acta 58, 5011–5029.
Iizasa, K., Sasaki, M., Matsumoto, K., Shiokawa, S., Tanahashi, M., onboard scientists, 2004. A first extensive hydrothermal field associated with Kuroko-type deposit in a Silicic Submarine caldera in a Nascent Rift Zone, Izu-Ogasawara (Bonin) arc, Japan. Oceans 2004 MTS/IEEE Conference: Techno-Ocean'04, pp. 991–996.
Imai, N., Terashima, S., Itoh, S., Ando, A., 1999. 1998 compilation of analytical data for five GSJ geochemical reference samples: the "instrumental analysis series". Geostand. Newslett. 23, 223–250.
Ishizuka, O., Yuasa, M., Usui, A., 1998. Low temperature hydrothermal activity on a back-arc seamount of the Izu-Ogasawara arc: submersible survey of the Nishi-Jokyo Seamount. JAMSTEC J. Deep Sea Res. 14, 245–268 (in Japanese with English abstract).
Konter, J.G., Jackson, M.G., 2012. Large volumes of rejuvenated volcanism in Samoa: evidence supporting a tectonic influence on late stage volcanism. Geochem. Geophys. Geosyst. 13, Q0AM04. http://dx.doi.org/10.1029/2011GC003974.
Kuhn, T., Bostick, B.C., Koschinsky, A., Halbach, P., Fendorf, S., 2003. Enrichment of Mo in hydrothermal Mn precipitates: possible Mo sources, formation process and phase associations. Chem. Geol. 199, 29–43.
Ling, H.-F., Jiang, S.-Y., Frank, M., Zhou, H.-Y., Zhou, F., Lu, Z.-L., Chen, X.-M., Jiang, Y.-H., Ge, C.-D., 2005. Differing controls over the Cenozoic Pb and Nd isotope evolution of deep-water in the central North Pacific Ocean. Earth Planet. Sci. Lett. 232, 345–361.
Ludwig, K.R., 2012. Isoplot 4.16: a geochronological toolkit for Microsoft Excel. Berkeley Geochronology Center Special Publication No. 6, p. 75.
Manheim, F.T., Lane-Bostwick, C.M., 1988. Cobalt in ferromanganese crusts as a monitor of hydrothermal discharge on the Pacific seafloor. Nature 335, 59–62.
Matthews, K.A., Murrell, M.T., Goldstein, S.J., Nunn, A.J., Norman, D.E., 2011. Uranium and thorium concentration and isotopic composition in five glass (BHVO-2G, BCR-2G, NKT-1G, T1-G, ATHO-G) and two powder (BHVO-2, BCR-2) reference materials. Geostand. Geoanal. Res. 35, 227–234.
Moorby, S.A., Cronan, D.S., Glasby, G.P., 1984. Geochemistry of hydrothermal Mn-oxide deposits from the SW Pacific island arc. Geochim. Cosmochim. Acta 48, 433–441.
Moore, W.S., Vogt, P.R., 1976. Hydrothermal manganese crusts from two sites near the Galapagos spreading axis. Earth Planet. Sci. Lett. 29, 349–356.
Nedjatpoor, M., Stoffers, P., Glasby, G.P., 1985. Influence of ageing effects on manganese nodule mineralogy. Neues Jahrb. Mineral. Mh. 5, 204–208.
Pelt, E., Chabaux, F., Innocent, C., Navarre-Sitchler, A.K., Sak, P.B., Brantley, S.L., 2008. Uranium–thorium chronometry of weathering rinds: rock alteration rate and paleo-isotopic record of weathering fluids. Earth Planet. Sci. Lett. 276, 98–105.
Robinson, L.F., Belshaw, N.S., Henderson, G.M., 2004. U and Th concentrations and isotope ratios in modern carbonates and waters from the Bahamas. Geochim. Cosmochim. Acta 68, 1777–1789.
Rogers, T.D.S., Hodkinson, R.A., Cronan, D.S., 2001. Hydrothermal manganese deposits from the Tonga-Kermadec Ridge and Lau Basin Region, Southwest Pacific. Mar. Georesour. Geotechnol. 19, 245–268.
Schulz, M.S., Hein, J.R., 1991. Petrography and chemistry of hydrothermal manganese oxyhydroxides from the Mariana and Izu-Bonin Volcanic arcs, West Pacific. U.S. Geol. Surv. Open File Rep. 91–557, p. 80.
Scott, M.R., Scott, R.B., Rona, P.A., Butler, L.W., Nalwalk, A.J., 1974. Rapidly accumulating manganese deposit from the Median Valley of the Mid-Atlantic Ridge. Geophys. Res. Lett. 1, 355–358.
Sun, S.-S., McDonough, W.F., 1989. Chemical and isotopic systematics of oceanic basalts: implications for mantle composition and processes. In: Saunders, A.D., Norry, M.J. (Eds.), Magmatism in the Ocean Basins. Geological Society Special Publication vol. 42. The Geological Society, London, pp. 313–345.
Sun, Z., Zhou, H., Yang, Q., Sun, Z., Bao, S., Yao, H., 2011. Hydrothermal Fe–Si–Mn oxide deposits from the Central and South Valu Fa Ridge, Lau Basin. Appl. Geochem. 26, 1192–1204.
Tanahashi, M., Shiokawa, S., Murayama, N., Takatori, R., 2006. A large hydrothermal sulphide deposit discovered in the Bayonnaise Knoll, Izu-Bonin back-arc rift. Shigen-Chishitsu 56, 185–196 (in Japanese with English abstract).
Tsuchida, S., Kumagai, H., Ishibashi, J., Watanabe, H., Kouzuma, F., 2001. Preliminary report of hydrothermalism and volcanism at the Kaikata Seamount. JAMSTEC J. Deep Sea Res. 18, 209–215 (in Japanese with English abstract).
Usui, A., Glasby, G.P., 1998. Submarine hydrothermal manganese deposits in the Izu-Bonin-Mariana arc: an overview. Island Arc 7, 422–431.
Usui, A., Nishimura, A., 1992. Submersible observations of hydrothermal manganese deposits on the Kaikata Seamount, Izu-Ogasawara (Bonin) Arc. Mar. Geol. 106, 203–216.
Usui, A., Nishimura, A., 1993. Manganese nodules, manganese crusts and limestones from the Tenpo Seamount, Nishi-Shichito Ridge, Izu-Ogasawara Arc. Proc. JAMSTEC Symp. Deep-Sea Res. 9, 117–131 (in Japanese with English abstract).
Usui, A., Someya, M., 1997. Distribution and composition of marine hydrogenetic and hydrothermal manganese deposits in the northwest Pacific. In: Nicholson, K., Hein, J.R., Bühn, B., Dasgupta, S. (Eds.), Manganese Mineralization: Geochemistry and Mineralogy of Terrestrial and Marine Deposits. Geological Society Special Publication vol. 119. The Geological Society, London, pp. 177–198.
Usui, A., Yuasa, M., Yokota, S., Nohara, M., Nishimura, A., Murakami, F., 1986. Submarine hydrothermal manganese deposits from the Ogasawara (Bonin) Arc, off the Japan Islands. Mar. Geol. 73, 311–322.
Usui, A., Mellin, T.A., Nohara, M., Yuasa, M., 1989. Structural stability of marine 10 Å manganates from the Ogasawara (Bonin) Arc: implication for low-temperature hydrothermal activity. Mar. Geol. 86, 41–56.